

Signatures of magnon hydrodynamics in an atomically-thin ferromagnet

Ruolan Xue^{1*†}, Nikola Maksimovic^{2*†}, Pavel E. Dolgirev², Li-Qiao Xia³, Ryota Kitagawa⁴, Aaron Müller⁵, Francisco Machado^{2,6}, Dahlia R. Klein^{3,7}, David MacNeill³, Kenji Watanabe⁸, Takashi Taniguchi⁸, Pablo Jarillo-Herrero³, Mikhail D. Lukin², Eugene Demler⁵, Amir Yacoby^{1,2*}

¹*John A. Paulson School of Engineering and Applied Sciences, Harvard University, Cambridge, MA, USA*

²*Department of Physics, Harvard University, Cambridge, MA, USA*

³*Department of Physics, Massachusetts Institute of Technology, Cambridge, MA, USA*

⁴*Department of Electrical and Electronic Engineering, Tokyo Institute of Technology, Tokyo, Japan*

⁵*Department of Physics, ETH Zürich, Zurich, Switzerland*

⁶*ITAMP, Harvard-Smithsonian Center for Astrophysics, Cambridge, MA, USA*

⁷*Department of Condensed Matter Physics, Weizmann Institute of Science, Rehovot, Israel*

⁸*Research Center for Functional Materials, National Institute for Materials Science, Tsukuba, Japan[†]*

(Dated: March 5, 2024)

Strong interactions between particles can lead to emergent collective excitations. These phenomena have been extensively established in electronic systems, but are also expected to occur for gases of neutral particles like spin waves, also known as magnons, in a ferromagnet. In a hydrodynamic regime where magnons are strongly interacting, they can form a slow collective density mode – in analogy to sound waves in water – with characteristic low-frequency signatures. While such a mode has been predicted in theory, its signatures have yet to be observed experimentally. In this work, we isolate atomically-thin sheets of ferromagnetic CrCl_3 where magnon interactions are strong, and develop a technique to measure its collective magnon dynamics via the quantum coherence of nearby Nitrogen-Vacancy (NV) centers in diamond. We find that the thermal magnetic fluctuations generated by CrCl_3 exhibit an anomalous temperature-dependence, whereby fluctuations increase upon decreasing temperature. Our analysis reveals that this anomalous trend is a consequence of the damping rate of a low-energy magnon sound mode which sharpens as magnon interactions increase with increasing temperature, providing a first glimpse of the magnon hydrodynamic regime.

I. INTRODUCTION

Modern quantum technologies are often based on magnetic materials, with applications ranging from non-boolean computing [1], to spin torque manipulation [2], to overcoming the Landauer limit of energy consumption [3, 4]. These technologies rely on the propagation of magnons – quanta of spin excitation – in magnetic materials [5]. A fundamental understanding of various magnon transport mechanisms is therefore crucial for the development, design, and operation of spintronic devices, especially those based on recently-discovered atomically-thin magnets [6].

Of particular interest is the realization of novel transport regimes. Typically, propagating magnons lose their momentum through collisions with the boundaries of the sample or the atomic lattice of the host material. A qualitatively different regime emerges when magnons collide predominantly with each other. Such a hydrodynamic regime is characterized by liquid-like flow in which transport is controlled by collisions within the fluid rather than its interactions with the host material. This hydrodynamic regime is further expected to exhibit a collective sound mode at energies lower than that of single magnon excitations [7–9].

In the solid state, hydrodynamic transport is an emerging field with growing evidence in electron systems [10–14], and even demonstrated practical value [15]. In theory, it has been suggested that a hydrodynamic regime could be realized in densely-populated and strongly interacting magnon gases, which exist in two-dimensional ferromagnets with highly isotropic spins [8, 9, 16, 17]. CrCl_3 , a magnetic insulator with relatively low single-ion anisotropy [18–23] and the potential to be isolated in atomically-thin form [24–26], is therefore an excellent candidate. However, it is challenging to measure collective dynamics of magnons in general, and even more so in atomically-thin materials because of their mesoscopic sample volumes and correspondingly small signals.

The latter difficulty could be naturally overcome using atomic-like defects such as nitrogen-vacancy (NV) centers in diamond, which are capable of detecting small magnetic field signals at the nanoscale [27, 28]. Previous studies demonstrated how proximal NV centers can be used to measure the dissipative magnetic susceptibility of a material through noise measurements in the GHz frequency range (also called T_1 relaxometry), via the fluctuation-dissipation theorem [29]. This technique has proven valuable for measuring not only critical phenomena near magnetic phase transitions [30], but also the spin diffusion constant in antiferromagnets [29, 31]. Here, we employ a magnetic noise sensing technique based on the dephasing rates (T_2) of NV centers in proximity to atomically-thin CrCl_3 . In contrast to T_1 relaxometry, Hahn-echo based T_2 dephasing spectroscopy provides direct access to the low frequency dynamics that are well

* ruolanxue@g.harvard.edu
nikola_maksimovic@fas.harvard.edu
yacoby@g.harvard.edu

† These authors contributed equally to this work.

below the frequencies of single magnons.

Our central finding is that the low-frequency magnetic noise in a CrCl₃ monolayer and thin bulk samples exhibits an enhancement with decreasing temperature. This observation is surprising given that usually thermal fluctuations generated by an ordered magnet are expected to freeze as temperature is reduced [32]. We show that the observed trend is a signature of a low-energy hydrodynamic magnon sound mode with anomalous damping rate set by magnon viscosity.

II. SENSING TECHNIQUES

Exfoliated CrCl₃ samples encapsulated by hBN are placed onto a bulk diamond surface with a uniform layer of NV centers implanted 55 nm beneath the surface (Fig. 1A). A sensing spot of about 640 nm diameter is selected within the NV layer using a focused green laser that can be spatially rastered around the CrCl₃ sample.

A layer of CrCl₃ hosts ferromagnetic nearest-neighbor exchange on a honeycomb lattice (Fig. 1B) [33]. Because the magnetization properties of exfoliated monolayers of this material have not previously been reported, we employ a conventional static field sensing technique to access the sample magnetization (Fig. 1C). We monitor the spatial variation of the NV spin state energy-splitting that directly reflects local static magnetic field (see supplement II.A). Through this procedure, the stray field generated by monolayer CrCl₃ can be imaged (Fig. 1D).

Access to low-energy spin dynamics is achieved through a quantum coherent sensing protocol. This procedure leverages phase-coherent pulses to evolve the NV spin state on the Bloch sphere (Fig. 1E). During the spin precession time over the course of this Hahn-echo sequence, dynamical magnetic noise leads to an exponential loss of state purity characterized by a dephasing rate $1/T_2$ (Fig. 1E inset). We isolate the sample-induced dephasing rate by subtracting the background rate taken off the sample (Fig. 1F and supplement II.C). To ensure that the signal obtained reflects the equilibrium noise, a variable delay between 1 μ s and 60 μ s was added between the initialization laser and the Hahn-echo sequence [34] (supplement V).

The sample-induced magnetic noise measures the dissipative component of the magnetic susceptibility of the material $\text{Im}[\chi(k, \omega)]$, subject to frequency and momentum filtering functions [35]. The probed frequency ω_{echo} is essentially set by the Hahn-echo sequence time, and the probed momentum k is strongly peaked at momenta given by the inverse of the NV-sample distance z_{NV} . The T_2 -signal is thus related to $\text{Im}[\chi(k_{\text{NV}}, \omega_{\text{echo}})]$ [35] (supplement X and V):

$$\frac{1}{TT_2} \propto \frac{\text{Im}[\chi(k_{\text{NV}}, \omega_{\text{echo}})]}{\omega_{\text{echo}}}, \quad (1)$$

where T is temperature. In this experiment, $k_{\text{NV}} \approx 1/z_{\text{NV}}$ with $z_{\text{NV}} = 65$ nm and $\omega_{\text{echo}} \sim 10 - 100$ kHz. Ac-

cess to these relatively short length-scales distinguishes NV noise measurements from conventional low-frequency probes of dynamical susceptibility [36]. Furthermore, in contrast to T_1 relaxometry, the frequency band of T_2 measurements is solely controlled by the pulse sequence, allowing robust access to low-frequency dynamics at any applied magnetic field.

III. RESULTS

A. Monolayer CrCl₃

The stray field generated by the sample can be interpreted as an indirect measurement of its magnetization (see supplement IV for a quantitative relationship) [24, 37]. Here we utilize this property to experimentally estimate the ferromagnetic transition temperature and the exchange constant of a monolayer CrCl₃ film. The monolayer sample is shown in Fig. 2A with the corresponding optical image and magnetic stray field map at 6 K. The stray field across the monolayer flake (Fig. 2B) decreases considerably upon raising temperature from 6 K to 15 K. The temperature-dependence of the integrated stray field across the sample indicates that the material undergoes a ferromagnetic-to-paramagnetic phase transition around $T_c = 12.5$ K (Fig. 2C) in agreement with previous measurements on epitaxially-grown monolayer CrCl₃ [24].

We extract the exchange interaction J by fitting the temperature-dependent stray field data within the ferromagnetic state to a self-consistent linearized spin wave theory (details see SI IV.x and VII) with two free parameters (Fig. 2C) – J , and an overall scale factor converting magnetization to stray field. The exchange constant we obtain ($J = 10.9 \pm 0.4$ K) agrees well with previous measurements on multilayer CrCl₃ [21]. The deviation between the model and experimental data above 12.5 K can be attributed to the failure of linearized spin-wave theory close to the transition temperature [38]. From the agreement between the model and experimental data within the ferromagnetic state, we conclude that dipolar interactions stabilize the ferromagnetic phase (see also supplement IX), and that magnons are the relevant elementary excitations below 12.5 K when modeling the spin dynamics of a monolayer CrCl₃.

While the static magnetic properties conform to a spin-wave model [21, 24], the observed spin dynamics, as measured by $1/T_2$, unveil peculiar behavior indicative of the existence of strong magnon interactions within the ferromagnetic state. These measurements are performed both with a 4 mT bias field normal to the sample plane and a 136 mT field along the NV axis 54° from normal (Fig. 3A).

At 4 mT, the noise exhibits sharp peaks close to the transition temperature as inferred from static field mea-

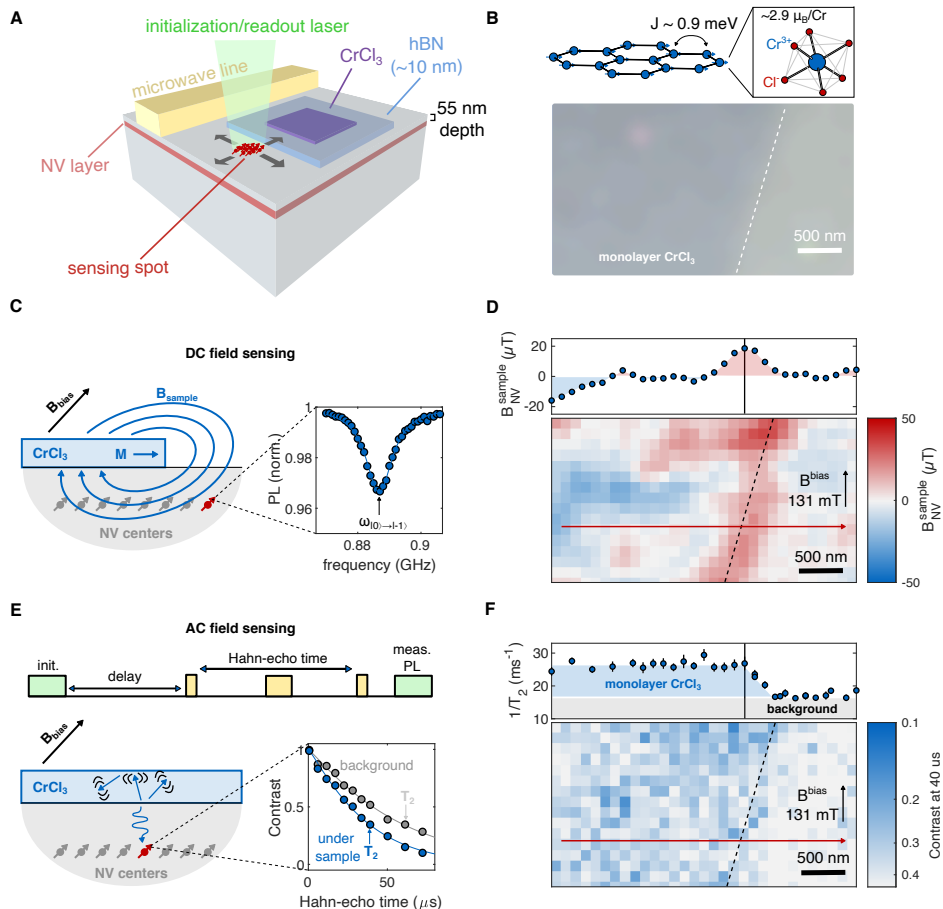


FIG. 1. CrCl_3 material properties and nitrogen-vacancy (NV) center sensing techniques. **A** CrCl_3 samples are placed on the surface of a diamond slab, which contains a uniform layer of shallow NV centers. A focused laser addresses a movable sensing spot in the NV layer. **B** Crystal structure of the monolayer CrCl_3 and its relevant magnetic exchange interaction along with an optical image of a region of a monolayer CrCl_3 . **C** Sensing protocol in which the static field along the NV quantization axis, with contributions from both the sample ($B_{\text{NV}}^{\text{sample}}$) and applied bias field ($B_{\text{NV}}^{\text{bias}}$), is measured via the magnetic resonance of the NV spin state $\omega_{0 \rightarrow -1}$ detected via optical photoluminescence (PL). **D** $B_{\text{NV}}^{\text{sample}}$ is isolated by rastering the sensing spot position across the sample and subtracting the bias field determined off the sample. This image was taken at 5.2 K with a 131 mT bias field applied 54° from surface normal. **E** AC field sensing is achieved by measuring the dephasing rate, $1/T_2$, of the NV centers under the Hahn-echo pulse sequence. T_2 is determined by fitting the Hahn-echo contrast to an exponential (supplement II.C). A variable delay between the initialization laser and measurement sequence was employed to ensure that the obtained signal reflects the equilibrium properties of the sample (see supplement VII). **F** An image of the Hahn-echo contrast at 40 μs evolution time taken under the same conditions as in **D**. Dark blue regions indicate faster NV dephasing. The line cut shows $1/T_2$ as obtained from a full fit of the Hahn-echo decay at each spatial point.

measurements. Subsequently, the noise level continues to rise with further cooling down to our lowest recorded temperature (Fig. 3A). A 136 mT magnetic field suppresses the features near the transition temperature, but only weakly affects the increasing noise trend with lowering temperature.

The peak in noise near the phase transition likely results from critical fluctuations [35]. The suppression of this feature for the stronger magnetic field could result from the explicit symmetry-breaking effect of the planar component of the applied field. The presence of two closely-spaced peaks appears to be non-generic (see supplement VI for measurements on another sample), point-

ing to spatial inhomogeneity in transition temperatures of a few percent on length scales of the sensing spot. Similar variation in transition temperatures has been observed previously in epitaxial CrCl_3 monolayers [24].

The increase of $1/T_2$ with decreasing temperature is a surprising observation given that, on general grounds, the magnetic noise in an ordered ferromagnet should monotonically decrease with decreasing T as thermal fluctuations become progressively more frozen [32]. We argue that this anomalous noise scaling is a signature of magnon hydrodynamics. At the temperatures of the experiment, the magnons comprise a dense gas, which produces noise at the NV location due to the trans-

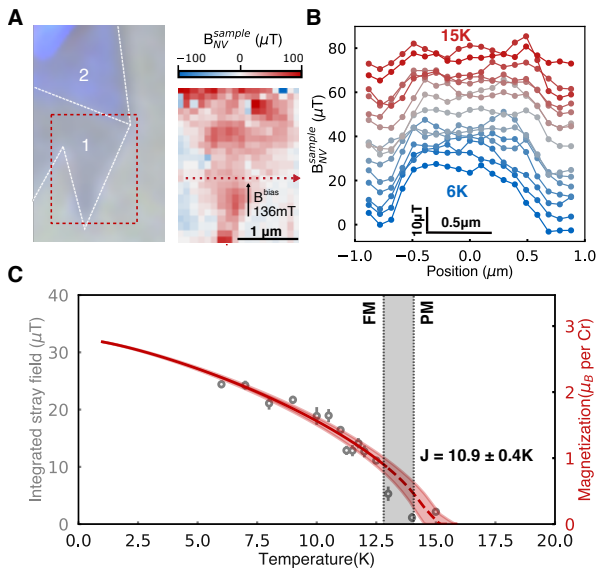


FIG. 2. Static magnetization properties of a monolayer CrCl₃. **A** Optical image containing a monolayer(1) and bilayer(2), alongside a stray field map taken on the monolayer with a 136 mT bias field applied 54° from the surface normal at 6 K. **B** Temperature-dependent stray field measurement across the monolayer flake as is indicated by the red line in **A**. **C** Integrated stray field over the area of the sample as a function of temperature. A sharp decrease in the integrated stray field upon raising temperature above 12.5 K indicates that the material undergoes a ferromagnetic-to-paramagnetic phase transition. The red line is a fit to our dipolar spin-wave model (supplement IX), from which we determine the ferromagnetic exchange constant, J .

port of density fluctuations of the gas through the nanoscale sensing region [31]. The magnons are so strongly-interacting in the monolayer CrCl₃ that the gas can form a low-energy long-lived collective sound mode, which both moves faster and becomes longer lived as temperature increases. This interaction-driven speed-up and linewidth narrowing counteracts the amplification of thermal fluctuations, ultimately leading to a suppression of noise with increasing temperature.

We first note that the $1/T_2$ signal is expected to be insensitive to single magnon excitations. To see this explicitly, we plot the magnon dispersion in monolayer CrCl₃ computed based on our linearized spin-wave theory in Fig. 3B. The NV center filters out momenta away from $k_{\text{NV}} \simeq 1/z_{\text{NV}}$. Magnons near k_{NV} have frequencies in the GHz range, which are highly off-resonant with the frequencies of the $1/T_2$ measurements (see inset of Fig. 3B).

Instead, the $1/T_2$ signal originates from density fluctuations of the magnon gas, as depicted in the momentum-space diagram in Fig. 3B [31]. These fluctuations are associated with magnon scattering processes with momentum transfer set by k_{NV} and frequency transfer set by ω_{echo} . At the typical temperatures of the experiment,

the thermal momentum of magnons q_{th} is significantly larger than k_{NV} . As such, the main contribution to density fluctuations at the NV location arises due to interactions of high-momentum thermal magnons (supplement XII). These thermal magnons are so high energy that the small anisotropy energy scales (dipolar, single-ion, and planar magnetic field) have little effect on their dispersion. They essentially obey a parabolic dispersion with the mass m set by the exchange interaction and an effective small pseudo-gap Δ , which originates from the weak effects of the anisotropy (Fig. 3B, Fig. S6).

These high-momentum thermal magnons in CrCl₃ are also predicted to strongly interact, and their interactions grow with increasing temperature. This can be deduced from the fact that the dominant exchange-mediated magnon-magnon interaction in this relatively isotropic spin system increases with momentum [17] and thus increases not only with magnon density n but also with the thermal momentum. Indeed, the corresponding mean free path for magnon-magnon exchange collisions $l_{\text{mfp}} \simeq (J/T)^{3/2}/(na) \sim T^{-5/2}$ [17], where a is the lattice constant, shrinks rapidly with increasing temperature. This crude estimate gives $l_{\text{mfp}} \simeq 18$ nm at $T = 5$ K and $l_{\text{mfp}} \simeq 3$ nm at $T = 10$ K, indicating that magnon-magnon interactions could dominate over all other scattering processes and put the magnon gas in a hydrodynamic regime over the length scale probed by the NV center, $k_{\text{NV}}l_{\text{mfp}} \lesssim 1$, even at $T = 5$ K.

In this case, the magnon gas forms a low-energy collective sound mode whose broadening due to finite lifetime spans frequencies down to those of the $1/T_2$ measurements (Fig. 3C). The sound mode has a linear dispersion set by the speed of sound v_s and decay rate set by the magnon viscosity μ . The spectral weight in the $1/T_2$ measurement has two opposing contributions as temperature increases from 5 K to 10 K. On the one hand, the magnon density increases with temperature (Fig. 3D) thereby increasing the overall strength of magnetic fluctuations. On the other hand, v_s and the sound lifetime both increase with increasing temperature, both of which contribute to the decreasing noise at low frequencies. In particular, in the high magnon density regime we operate in, with $T \gg \Delta$, we find that the sound velocity is set by the pseudogap Δ : $v_s^2 \approx (\Delta/m) \log|(\Delta/T)|$ (supplement XIII.B). For the magnon viscosity μ , we get $\mu \propto q_{\text{th}} n l_{\text{mfp}} \sim 1/T$, where $n \sim T$ and $q_{\text{th}} \sim T^{1/2}$ (see also supplement XIV.A).

Taking into account these two competing effects, we find a quantitative relationship between the $1/T_2$ noise and the properties of the sound mode ($1/(TT_2) \propto \mu/v_s^4$); more precisely,

$$\frac{1}{TT_2} \simeq C \frac{1}{z_{\text{NV}}^4} \frac{\mu}{\Delta^2 \log^2(\Delta/T)}. \quad (2)$$

Here C is a constant (see supplement VI.D). The exchange-driven magnon viscosity is expected to scale as $1/T$ (Fig. 3D), producing a $1/T_2$ signal that decreases with increasing T and providing an interpretation to

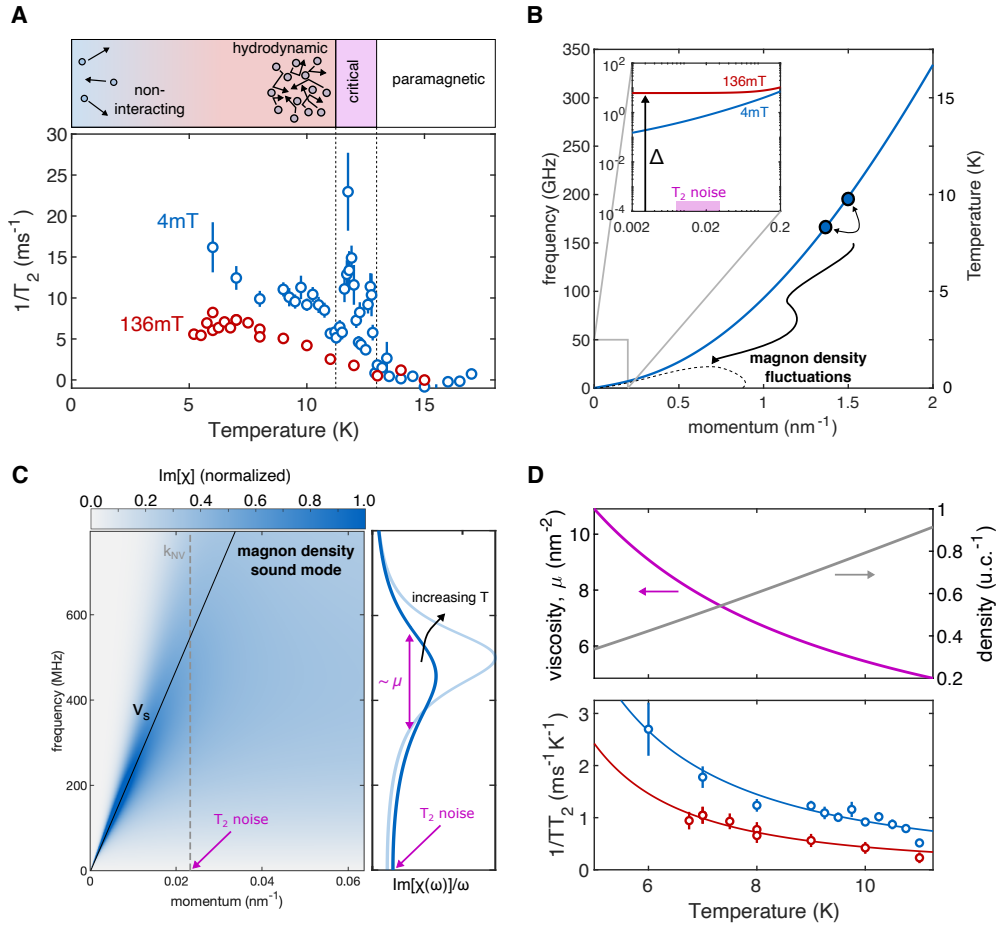


FIG. 3. Dephasing spectroscopy of a monolayer CrCl_3 and relation to magnon dynamics. **A** Sample-induced $1/T_2$ dephasing rate, averaged over the area of the monolayer sample, at both 4 mT external field normal to the sample and 136 mT tilted 54° from the normal. **B** Calculated magnon dispersion along the Γ - K' direction, at both applied magnetic fields as in the experiment. The inset shows a zoom-in with a label of the relevant frequency and momenta of the T_2 noise measurements (pink square). The dispersion is essentially parabolic with an effective gap Δ set by anisotropy terms. The right axis is the energy scale plotted in the unit of temperature. Our measurements occur between 5 and 15 K. Although the T_2 sensing frequency is off-resonant with the relevant magnons, magnon scattering processes produce density fluctuations resulting in low-frequency noise apparent in T_2 measurements. **C** Modeled $\text{Im}[\chi]$ of the magnon sound mode in a hydrodynamic regime. A linecut at k_{NV} depicts how T_2 noise (related to $\text{Im}[\chi]/\omega$ via Eq. (1)) is proportional to the viscous damping rate, μ , of the sound mode. **D** Top panel shows calculated magnon density $n(T)$ and exchange-driven magnon viscosity $\mu(T)$, which is shown to decrease with increasing T . The bottom panel shows a fit to the data based on our phenomenological theory in Eq. (2), allowing us to extract the magnon viscosity μ as well as the gap Δ .

the experiment. Note that if the dominant magnon interactions were contact rather than exchange mediated, $\mu \sim T$, and the opposite trend would result (supplement XIV.A). Based on our model, the increase in applied field from 4 mT to 135 mT enhances Δ by roughly a factor of two, and thus the noise given by Eq. (2) is expected to decrease also by about a factor of two.

This phenomenological theory produces excellent qualitative agreement with our $1/T_2$ measurements (Fig. 3D). The agreement further allows us to extract two physical quantities of the system: viscosity μ and pseudogap Δ via a fit (supplement VI.D). We obtain $C\mu T/z_{\text{NV}}^4 = 55 \pm 10 \text{ K}^2/\text{ms}$ and $\Delta = 1.2 \pm 0.2 \text{ K}$ at 4 mT; $C\mu T/z_{\text{NV}}^4 = 40 \pm 10 \text{ K}^2/\text{ms}$ and $\Delta = 1.7 \pm 0.7 \text{ K}$ at 136 mT. From these fit

parameters, and using $z_{\text{NV}} = 65 \text{ nm}$, we obtain an estimate of the two-dimensional viscosity of the magnon gas as varying between $1\text{-}2 \times 10^{-10} \text{ kg/s}$ under these experimental conditions (see supplement VI.D).

In agreement with the prediction of our theory, a 30-fold enhancement of magnetic field reduces $1/T_2$ by roughly a factor of two, and similar viscosity values are obtained at both magnetic fields. Within error bars, quantitative agreement is found on a separate monolayer sample (supplement VI.D).

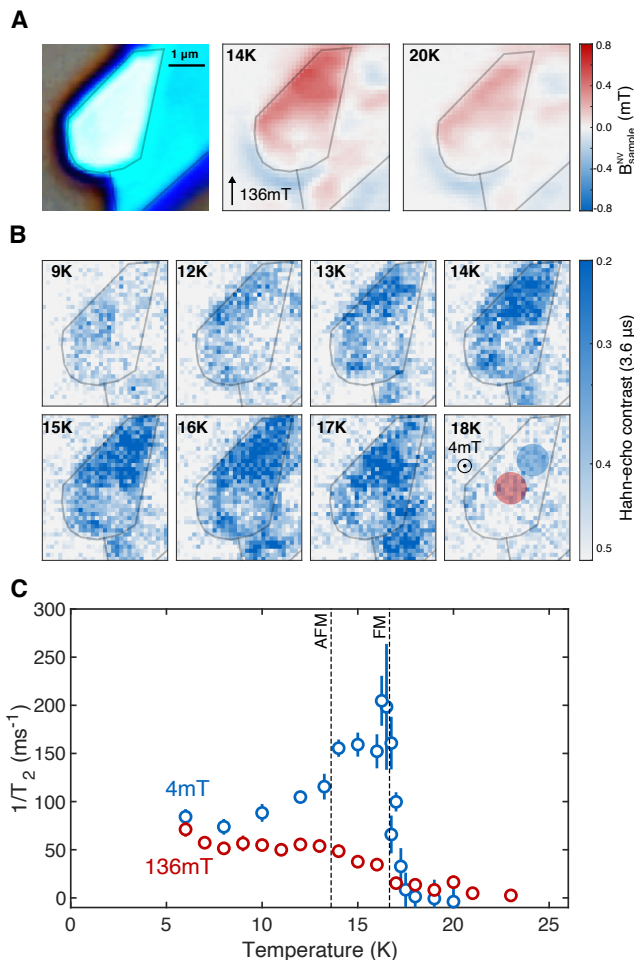


FIG. 4. Static magnetization and dephasing spectroscopy of thin bulk CrCl₃. **A** Optical image of thin bulk CrCl₃ along with stray field measurements at 14 K and 20 K with a 136 mT field applied 54° from normal to the plane. The grey contour indicates the edge of the sample. **B** Spatial images of the dephasing spectroscopy result with a 4 mT out of plane field. The color bar represents the Hahn-echo NV contrast with a total evolution time of 3.6 μs. **C** 1/T₂ measurements versus temperature at points on the sample denoted in panel **B**.

B. Bulk CrCl₃

Here we extend our measurements to a multilayer stack of CrCl₃ of 26 nm thickness where the system can be thought of as CrCl₃ monolayers that are weakly antiferromagnetically coupled [20]. We aim to investigate how this coupling affects the spin dynamics in comparison to the monolayer.

From the perspective of static magnetization, it is known that AFM coupling between layers induces an AFM ground state with $T_{\text{AFM}} = 14$ K [20, 25, 39]. Ferromagnetism within the 2D sheets appears to form at a slightly higher temperature ($T_{\text{FM}} \approx 17$ K) [20]. In our measurements, an applied field of 135 mT induces a finite stray field around the sample (Fig. 4A), the magnitude

of which at 14 K is approximately 50% of that expected from a fully polarized sample. This implies a cancellation effect of the magnetization between opposing layers in accordance with our expectations. The finite sample magnetization originates from the fact that the magnetic field is comparable to the interlayer exchange, and thus cants the spins between layers [20].

The general trend observed in the temperature-dependent dephasing images (Fig. 4B) is that the sample-induced magnetic noise abruptly rises upon cooling from 18 K to 17 K close to the anticipated intralayer ferromagnetic transition. The noise then gradually decreases between 14 K and 9 K. Further insight is gained through temperature-dependent measurements of 1/T₂ in specific regions of the sample (Fig. 4C), where at 4 mT, 1/T₂ shows a sharp enhancement upon cooling through the FM transition temperature, and a sharp drop across the AFM phase transition. 1/T₂ continues slowly decreasing upon cooling further until very low temperatures where we observe the plateauing of this behavior, with the lowest temperature suggesting its eventual reversal. The features associated with the phase transitions — the plateau between the AFM and FM transitions, and the broad tail below the AFM transition — are quenched by a 136 mT magnetic field, but the low-temperature behavior is essentially unaffected. The weak increase of 1/T₂ with decreasing temperature, most notably at 136 mT, could indicate that the interpretation applied to an isolated monolayer to some degree extends to the multilayer case.

Notably, however, the observed 1/T₂ signal in the AFM state is much smaller than that expected of additive monolayers. The 26 nm thickness corresponds to roughly 45 layers, where we expect 1/T₂ ≈ 200 ms⁻¹ using the measured viscosity of monolayer and integrating Eq. (2) across the depth of the 26 nm thick bulk sample. The comparatively low noise signal observed in the bulk antiferromagnet indicates that interlayer AFM coupling has a non-trivial influence on the properties of the asserted magnon sound mode within the 2D layers. A quantitative investigation of this effect is left to future work.

IV. DISCUSSION

In this work, we measure the dissipative magnetic response of atomically-thin CrCl₃ based on the coherence of nearby NV centers in diamond. The central experimental finding is the observation of a continuous enhancement of magnetic noise with decreasing temperature that is only weakly suppressed by 30-fold increase in the externally applied magnetic field. The data are interpreted as a signature of exchange-collision induced hydrodynamic magnon transport, in which the NV center is employed as a magnon viscometer. We further corroborate this interpretation by discussing in the supplement how other mechanisms, including the damping of single magnon [40, 41], magnetic vortices [33], magnetization

tunneling [42], exotic magnetic particles [43], and spin glass physics [44, 45] all fail to fully capture the experimental phenomenology (see supplement XV.A). While we do not fully account for a potential coupling of the sample signal to the spin bath of the background (primarily P1 centers [46, 47]), our analysis in supplement XV.A indicates that such a coupling is unlikely to be the origin of the anomalous noise trend. We also note that the microscopic calculation of the hydrodynamic transport coefficients of a strongly-interacting magnon gas presents a challenge to future theory.

This work provides a first glimpse of hydrodynamic magnons, and in particular evidence for viscous damping of a low-lying magnon sound mode. We also provide concrete predictions for the sound mode velocity, motivating future efforts towards its direct detection, as well as ultimately its potential application in magnon-based devices. Finally, the NV-based sensing protocol introduced here may be further extended to study magnetic dynamics in a wide range of materials.

V. ACKNOWLEDGMENTS

The authors would like to thank I. Esterlis and J. Rodriguez-Nieva for fruitful discussions, and M. Tschudin for assistance with the experiment. This work is supported by the Quantum Science Center (QSC), a National Quantum Information Science Research Center of the U.S. Department of Energy (DOE). A. Y. is also partly supported by the Gordon and Betty Moore Foundation through Grant GBMF 9468, and by the U.S. Army Research Office (ARO) MURI project under grant number W911NF-21-2-0147. R. X. is also partly supported by the Army Research Office under Grant numbers: W911NF-22-1-0248. N.M. is supported by an ap-

pointment to the Intelligence Community Postdoctoral Research Fellowship Program at Harvard University administered by Oak Ridge Institute for Science and Education. The work of P.E.D. is sponsored by the Army Research Office and was accomplished under Grant Number W911NF-21-1-0184. A.M. and E.D. are supported by the SNSF project 200021_212899 and the Swiss State Secretariat for Education, Research and Innovation (SERI) under contract number UeM019-1. FM acknowledges support from the NSF through a grant for ITAMP at Harvard University. PJH acknowledges support by the 2DMAGIC MURI FA9550-19-1-0390, the National Science Foundation (DMR-1809802), the STC Center for Integrated Quantum Materials (NSF grant no. DMR-1231319), the Gordon and Betty Moore Foundation's EPiQS Initiative through grant GBMF9463, and the Ramon Areces Foundation.

AUTHOR CONTRIBUTIONS

R.X., N.M., and A.Y. conceived the experiment. R.X., N.M., and R.K. performed the experiment and data analysis. P.E.D., A.M., and F.M. developed the theoretical interpretation of the experiment, with critical input from A.Y., E.D., and M.D.L. L-Q.X. and R.X. fabricated the samples. D.R.K. and D.M. grew and characterized the CrCl_3 crystals. K.W. and T.T. provided the hBN crystals. All authors contributed to the writing of the manuscript.

DECLARATIONS

The authors declare no conflicts of interest. Raw data and analysis code are available upon reasonable request.

-
- [1] G. Csaba, A. Papp, and W. Porod, *Journal of Applied Physics* **115** (2014).
 - [2] N. Locatelli, V. Cros, and J. Grolier, *Nature materials* **13**, 11 (2014).
 - [3] A. Bérut, A. Arakelyan, A. Petrosyan, S. Ciliberto, R. Dillenschneider, and E. Lutz, *Nature* **483**, 187 (2012).
 - [4] R. Cuykendall and D. R. Andersen, *Optics Letters* **12**, 542 (1987).
 - [5] A. V. Chumak, V. I. Vasyuchka, A. A. Serga, and B. Hillebrands, *Nature physics* **11**, 453 (2015).
 - [6] K. S. Burch, D. Mandrus, and J.-G. Park, *Nature* **563**, 47 (2018).
 - [7] K. Michel and F. Schwabl, *Physik der kondensierten Materie* **11**, 144 (1970).
 - [8] G. F. Reiter, *Physical Review* **175**, 631 (1968).
 - [9] J. F. Rodriguez-Nieva, D. Podolsky, and E. Demler, *Physical Review B* **105**, 174412 (2022).
 - [10] J. A. Sulpizio, L. Ella, A. Rozen, J. Birkbeck, D. J. Perello, D. Dutta, M. Ben-Shalom, T. Taniguchi, K. Watanabe, T. Holder, *et al.*, *Nature* **576**, 75 (2019).
 - [11] L. Levitov and G. Falkovich, *Nature Physics* **12**, 672 (2016).
 - [12] D. Bandurin, I. Torre, R. K. Kumar, M. Ben Shalom, A. Tomadin, A. Principi, G. Auton, E. Khestanova, K. Novoselov, I. Grigorieva, *et al.*, *Science* **351**, 1055 (2016).
 - [13] J. Crossno, J. K. Shi, K. Wang, X. Liu, A. Harzheim, A. Lucas, S. Sachdev, P. Kim, T. Taniguchi, K. Watanabe, *et al.*, *Science* **351**, 1058 (2016).
 - [14] P. J. Moll, P. Kushwaha, N. Nandi, B. Schmidt, and A. P. Mackenzie, *Science* **351**, 1061 (2016).
 - [15] J. Geurs, Y. Kim, K. Watanabe, T. Taniguchi, P. Moon, and J. H. Smet, *arXiv preprint arXiv:2008.04862* (2020).
 - [16] F. Schwabl and K. Michel, *Physical Review B* **2**, 189 (1970).
 - [17] F. J. Dyson, *Physical review* **102**, 1217 (1956).
 - [18] A. Narath, *Physical Review* **131**, 1929 (1963).
 - [19] M. Kostryukova and L. Luk'yanova, *Soviet Journal of Experimental and Theoretical Physics* **34**, 391 (1972).

- [20] M. A. McGuire, G. Clark, K. Santosh, W. M. Chance, G. E. Jellison Jr, V. R. Cooper, X. Xu, and B. C. Sales, *Physical Review Materials* **1**, 014001 (2017).
- [21] H. H. Kim, B. Yang, S. Li, S. Jiang, C. Jin, Z. Tao, G. Nichols, F. Sfigakis, S. Zhong, C. Li, *et al.*, *Proceedings of the National Academy of Sciences* **116**, 11131 (2019).
- [22] D.-H. Kim, K. Kim, K.-T. Ko, J. Seo, J. S. Kim, T.-H. Jang, Y. Kim, J.-Y. Kim, S.-W. Cheong, and J.-H. Park, *Physical review letters* **122**, 207201 (2019).
- [23] D. MacNeill, J. T. Hou, D. R. Klein, P. Zhang, P. Jarillo-Herrero, and L. Liu, *Physical review letters* **123**, 047204 (2019).
- [24] A. Bedoya-Pinto, J.-R. Ji, A. K. Pandeya, P. Gargiani, M. Valvidares, P. Sessi, J. M. Taylor, F. Radu, K. Chang, and S. S. Parkin, *Science* **374**, 616 (2021).
- [25] X. Cai, T. Song, N. P. Wilson, G. Clark, M. He, X. Zhang, T. Taniguchi, K. Watanabe, W. Yao, D. Xiao, *et al.*, *Nano letters* **19**, 3993 (2019).
- [26] D. R. Klein, D. MacNeill, Q. Song, D. T. Larson, S. Fang, M. Xu, R. A. Ribeiro, P. C. Canfield, E. Kaxiras, R. Comin, *et al.*, *Nature Physics* **15**, 1255 (2019).
- [27] R. Schirhagl, K. Chang, M. Loretz, and C. L. Degen, *Annual review of physical chemistry* **65**, 83 (2014).
- [28] C. L. Degen, F. Reinhard, and P. Cappellaro, *Reviews of modern physics* **89**, 035002 (2017).
- [29] H. Wang, S. Zhang, N. J. McLaughlin, B. Flebus, M. Huang, Y. Xiao, C. Liu, M. Wu, E. E. Fullerton, Y. Tserkovnyak, *et al.*, *Science advances* **8**, eabg8562 (2022).
- [30] N. J. McLaughlin, C. Hu, M. Huang, S. Zhang, H. Lu, G. Q. Yan, H. Wang, Y. Tserkovnyak, N. Ni, and C. R. Du, *Nano Letters* **22**, 5810 (2022).
- [31] B. Flebus and Y. Tserkovnyak, *Physical Review Letters* **121**, 187204 (2018).
- [32] C. P. Slichter, *Principles of magnetic resonance*, Vol. 1 (Springer Science & Business Media, 2013).
- [33] X. Lu, R. Fei, L. Zhu, and L. Yang, *Nature communications* **11**, 4724 (2020).
- [34] X.-Y. Zhang, T. K. Graham, Y.-X. Wang, H. Bae, N. Delgado, Z.-C. Wang, J. Regner, K. Watanabe, T. Taniguchi, M. Jung, *et al.*, arXiv preprint arXiv:2312.08476 (2023).
- [35] F. Machado, E. A. Demler, N. Y. Yao, and S. Chatterjee, *Physical Review Letters* **131**, 070801 (2023).
- [36] C. Topping and S. Blundell, *Journal of Physics: Condensed Matter* **31**, 013001 (2018).
- [37] L. Rondin, J.-P. Tetienne, T. Hingant, J.-F. Roch, P. Maletinsky, and V. Jacques, *Reports on progress in physics* **77**, 056503 (2014).
- [38] P. Bruno, *Phys. Rev. B* **43**, 6015 (1991).
- [39] N. Bykovetz, A. Hoser, and C. Lin, *AIP Advances* **9** (2019).
- [40] M. Sparks, R. Loudon, and C. Kittel, *Physical Review* **122**, 791 (1961).
- [41] C. Jermain, S. Aradhya, N. Reynolds, R. Buhrman, J. Brangham, M. Page, P. Hammel, F. Yang, and D. Ralph, *Physical Review B* **95**, 174411 (2017).
- [42] S. Vitale, A. Cavalleri, M. Cerdonio, A. Maraner, and G. A. Prodi, *Journal of Applied Physics* **76**, 6332 (1994).
- [43] R. Dusad, F. K. Kirschner, J. C. Hoke, B. R. Roberts, A. Eyal, F. Flicker, G. M. Luke, S. J. Blundell, and J. S. Davis, *Nature* **571**, 234 (2019).
- [44] W. Reim, R. Koch, A. Malozemoff, M. Ketchen, and H. Maletta, *Physical review letters* **57**, 905 (1986).
- [45] J. Quilliam, S. Meng, C. Mugford, and J. Kycia, *Physical review letters* **101**, 187204 (2008).
- [46] E. Bauch, S. Singh, J. Lee, C. A. Hart, J. M. Schloss, M. J. Turner, J. F. Barry, L. M. Pham, N. Bar-Gill, S. F. Yelin, and R. L. Walsworth, *Phys. Rev. B* **102**, 134210 (2020).
- [47] B. L. Dwyer, L. V. Rodgers, E. K. Urbach, D. Bluvstein, S. Sangtawesin, H. Zhou, Y. Nassab, M. Fitzpatrick, Z. Yuan, K. De Greve, *et al.*, *PRX Quantum* **3**, 040328 (2022).